



OPEN

Novel estimation technique for the carrier-to-noise ratio of wireless medical telemetry using software-defined radio with machine-learning

Ishida Kai

In this study, we developed a novel machine-learning model to estimate the carrier-to-noise ratio (CNR) of wireless medical telemetry (WMT) using time-domain waveform data measured by a low-cost software-defined radio. With automatic estimation of CNR, the management of the electromagnetic environment of WMT can be made easier. Therefore, we proposed a machine-learning method for estimating CNR. According to the performance evaluation results by 5-segment cross-validation on 704 types of measured data, CNR was estimated with 99.5% R-square and 0.844 dB mean absolute error using a gradient boosting regression tree. The gradient boosting decision tree classifiers predicted if the CNR exceeded 30 dB with 99.5% accuracy. The proposed method is effective for investigating electromagnetic environments in clinical settings.

Wireless medical telemetry (WMT) is a typical medical device that continuously monitors a patient's physiological signs, such as heart rate. As WMT uses wireless communications, seamless communication is needed for patient monitoring. According to Electromagnetic Compatibility Conference Japan (EMCC) survey in 2021, about 80% of hospitals have introduced WMT, of which 60% are managing electromagnetic environments¹.

Notably, managing WMT frequency band is necessary in establishing a good WMT reception². For measuring the electromagnetic environment, we can detect poor receptions, electromagnetic interference (EMI) caused by various kinds of electrical devices, and malfunction of radio-receiving equipment to evaluate the electromagnetic environment³. A carrier-to-noise ratio (CNR), defined as the ratio of the received modulated carrier signal power C to the received noise power N after the receiver filters, is a criterion for the communication quality of WMT. A CNR of at least 15–20 dB is required for the minimum reception of WMT⁴. To achieve good reception, the manufacturer recommended a CNR of more than 30 dB⁵. The CNR is obtained by subtracting the background noise (BGN) power from the WMT signal power in its usage frequency. The degradation of WMT signal power may occur either by locating the transmitter at a null point or far away from the receiving antenna or the aging degradation of radio frequency components, which include receiving antennas, coaxial cables, connectors, and amplifiers⁶. However, electrical devices, especially switched-mode power supplies installed in light-emitting diode (LED) devices, may radiate unwanted emissions and increase BGN⁷. In addition, to promote the safe introduction and operation of WMT, it is necessary to consider effective frequency allocations, range of access, invasive radio waves from out-of-hospitals, and interference by intermodulation^{8–10}. Other wireless communication systems, such as real-time detection systems for dementia, may interfere with WMT because these devices use the same frequency band of WMT and are widely introduced in hospitals¹¹.

However, it is difficult to determine only BGN because hospitals generally use WMT transmitters for patient monitoring, whose power are hard to put off. Therefore, actual CNR is hard to measure in clinical settings. Unfortunately, there is a lack of interest in the electromagnetic compatibility (EMC) of WMT in most hospitals. Over 50% of hospitals do not have planned countermeasures for EMI, even with 20% of them having experienced EMI troubles with WMT¹. However, only 10% of hospitals have conducted periodic quantitative investigations of WMT because only a few staff in most hospitals have adequate skills or experience regarding EMC. Moreover, it is challenging to introduce a specific measuring device for the evaluation of EMC, such as a spectrum analyzer, in

Department of Medical Engineering, Faculty of Health Sciences, Junshin Gakuen University, 1-1-1 Chikushigaoka, Minami-ku, Fukuoka, Fukuoka 815-8510, Japan. email: gishikai310@gmail.com

most hospitals because of its cost. A simplified spectrum analysis function was installed in a WMT receiver, which measures the amplitude of received signals and/or electromagnetic noise in each WMT frequency channel¹². However, this function cannot operate during patient monitoring. Therefore, it is desirable to establish a novel, easier, and cost-effective technique for evaluating EMC in clinical settings.

In this study, we investigated a machine-learning technique to estimate the CNR of WMT to establish a novel simplified, automated, and low-cost evaluation method.

Concept of our approach

Figure 1 shows the time-domain envelopes of the WMT signal. The CNR of both WMT signals is approximately 21 dB, but the amplitudes of both carrier signal and BGN differ. The amplitude of carrier signal (a) is -90 dBm and (b) is -86 dBm, and the amplitude of BGN (a) is -111 dBm and (b) is -107 dBm. Our proposed method estimates CNR by a single measurement and provides CNR values using these waveforms. As described earlier, both the WMT signal and BGN should be measured severally in these cases to calculate CNR. We investigated the acquiring features of time-domain waveforms using signal processing for machine learning.

We employed a low-cost software-defined radio (SDR) device as a receiver like a spectrum analyzer to provide an easier and low-cost method as much as possible. SDR is a radio communication system in which traditionally implemented components in hardware (e.g., mixers, filters, amplifiers, modulators/demodulators, and detectors) are instead implemented using software on a personal computer or an embedded system¹³. We estimated the CNR of WMT using time-domain waveform data measured by the SDR receiver and machine-learning techniques. We considered this approach as adequate for machine learning.

Data collection and labeling

We obtained the time-domain waveform of the WMT signal measured by a low-cost SDR receiver to structure datasets for machine-learning. We used a USB dongle-type SDR receiver (RTL2832U, RTL-SDR) with a resolution of 8-bit and a cost of approximately \$30. This SDR was connected to a personal computer. Figure 2 shows the measurement setup. The WMT transmitter was placed in a transverse electromagnetic (TEM) cell to extract carrier signals only via the variable attenuator¹⁴. We used two types of transmitters made by different manufacturers: ZS-610P (Nihon-Kohden Co., Ltd.) and LX-8100 (Fukuda Denshi Co., Ltd.). The SDR transmitter (ADALM-Pluto, Analog Devices) connected with a personal computer for control was used as a signal generator which generated Gaussian noise in the 400 MHz band. We considered Gaussian noise to be BGN. According to a previous report, WMT employs a narrow band reception of 12.5 kHz; hence, most unwanted emissions generated from LED devices are band-limited to this bandwidth and are approximated as Gaussian noise⁷. Both the WMT signal and Gaussian noise were inputs to the SDR receiver through a hybrid coupler. The measurement was conducted at a measurement frequency of 429.325 MHz (using Japanese WMT channel number 3007¹⁵), the sample rate was 1 MHz, and the number of samples for one measurement was 2,000,000. Each measured data comprising 2,000,000 points was separated into 10,000 points. We obtained 708 conditions of data that were changed amplitudes of both WMT signal and Gaussian noise using a variable attenuator to replicate the various reception levels. Figure 3 shows the CNR distributions of the measured data. The CNR values ranged from 1 to 58 dB.

In this study, we used supervised learning, and labeled actual CNR values for each measured data. First, we measured the WMT signal and BGN power at each amplitude level using a real spectrum analyzer (RSA306B, Tektronix). The CNR was calculated from these WMT and BGN levels. We labeled a CNR of more than 30 dB or not to each data.

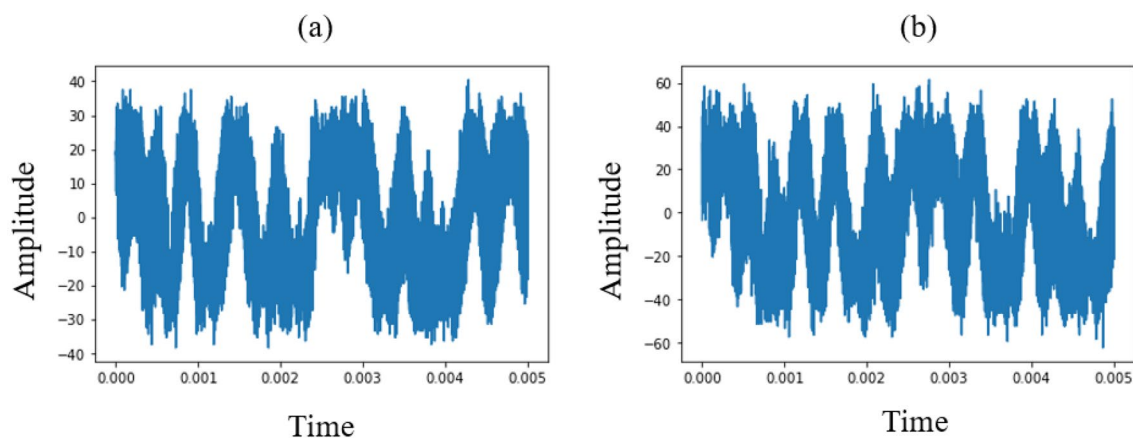


Figure 1. Time-domain envelopes of the WMT signal.

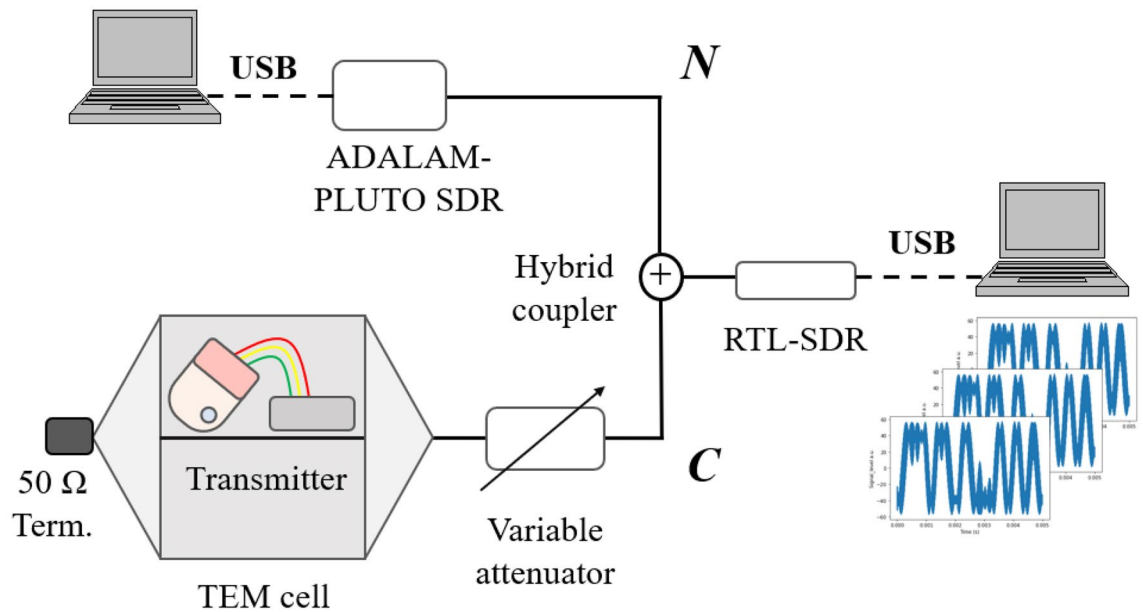


Figure 2. Measurement setup for WMT signals.

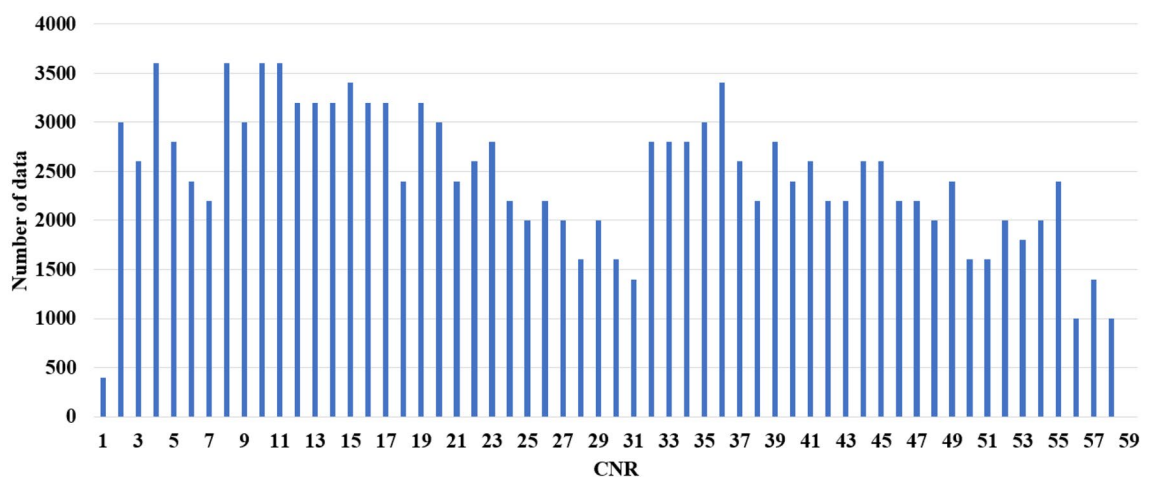


Figure 3. CNR distribution of the measured data.

Features, regressors, classifiers, and evaluation indexes for supervised machine-learning

In this study, we used 31-dimensional features calculated from the measured data by signal processing. Figure 4 shows the schematics of signal processing. First, we used simple moving averages with an interval of 300 points along the separated measured time-domain waveforms to detect envelope waves to obtain low-frequency features. We obtained the mean, standard deviation, minimum (Min), maximum (Max), and gradient calculated from envelope waves, which are between one-third and two-thirds of the total time. Moreover, the number of peaks of envelope waves between one-eighth and six-eighth of the time was calculated for each feature. In addition, we used the Butterworth filter, whose passband edge frequency was 10 Hz and stopband edge frequency was 40 Hz, to measure the time-domain waveforms for obtaining high-frequency features. Z-score normalization was used for this filtered data. Next, a fast Fourier transform was used to calculate the frequency spectra. We used librosa library, a Python module for audio and music processing, to obtain a chromagram, zero-crossing rate, spectral centroid, spectral bandwidth, roll-off frequency, and 1–20 coefficients of the Mel-frequency cepstral coefficients (MFCCs)^{16,17}.

Candidates for the regressors and classifiers are k-nearest neighbor (KNN)¹⁸, logistic regression (LR, classifier only)¹⁹, decision tree (DT, classifier only)²⁰, random forest (RF)²¹, support vector machine (SVM)²², gradient boosting regression tree (GBRT) and decision tree (GBDT)²³, ensemble algorithm (Adaboost)²⁴, and two-layer neural network (NN)²⁵. We tuned hyper parameters in these regressors and classifiers; number of neighbors in KNN, maximum depth, maximum leaf nodes and minimum sample leaf in DT, number of trees and maximum depth in RF and GBRT, the radius basis function kernel (γ) and regularization parameter (C) in SVM,

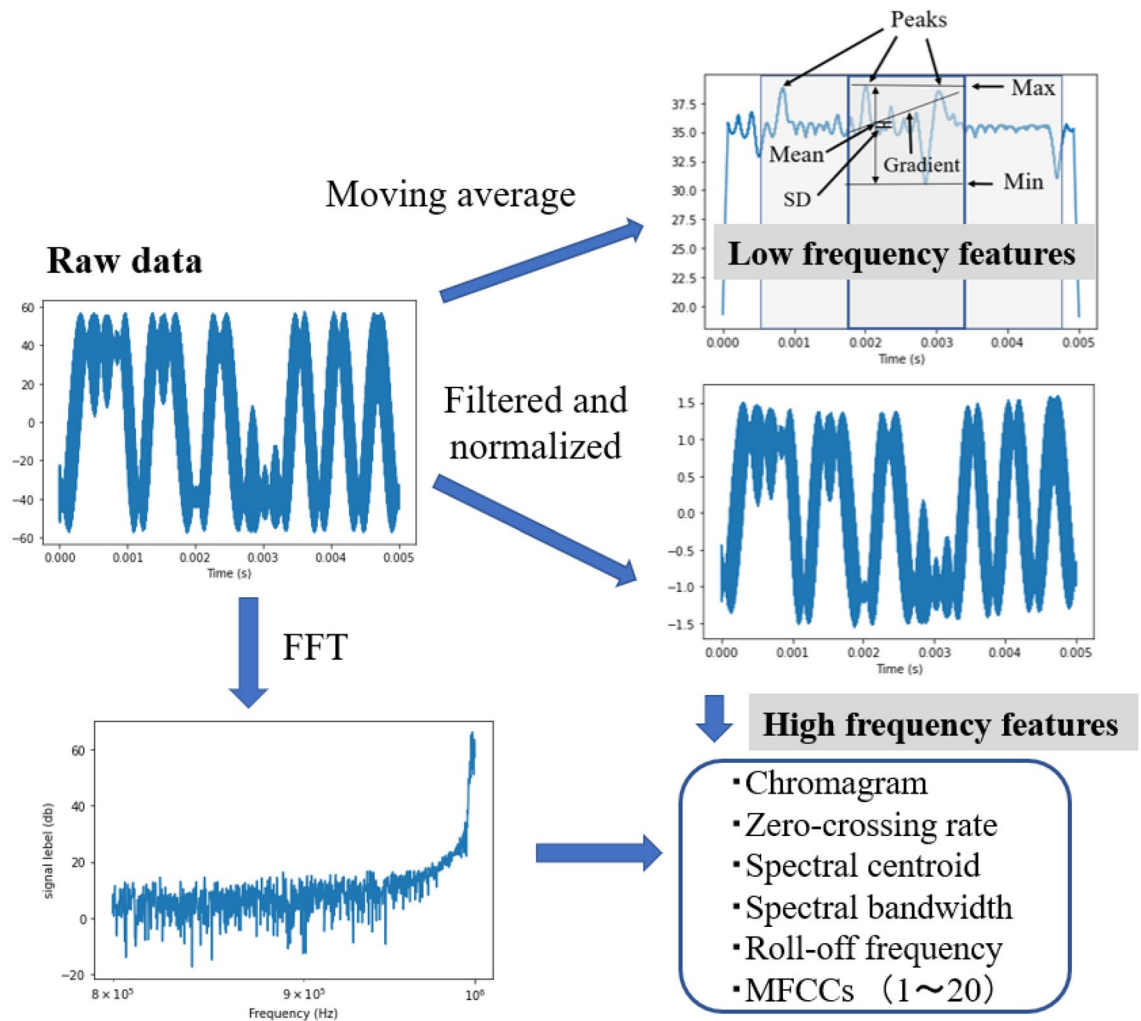


Figure 4. Schematics of signal processing for acquiring features.

learning rate and number of boost round in GBDT, number of trees, maximum depth and learning rate in Ada-Boost and epoch size, batch size and learning rate in NN. After which we selected the best parameters.

To avoid overtraining, we employed a 5-segment cross-validation for regression analysis and Stratified Group K-Fold (K=5) for classification. In regression analysis, R^2 score, which is the coefficient of determination and mean absolute error (MAE), was used as a criterion for evaluating the performance of supervised learning. In contrast, accuracy and recall were used in the classification instead. Generally, accuracy, true positive rate (TPR), true negative rate (TNR), false-negative rate (FNR), and false-positive rate (FPR) are used as criteria for evaluating the performance of supervised machine-learning algorithms, as defined by the following formulas:

$$\text{Accuracy} = (\text{TP} + \text{TN}) / (\text{TP} + \text{FP} + \text{TN} + \text{FN}) \tag{1}$$

$$\text{TPR} = \text{Recall} = \text{TP} / (\text{TP} + \text{FN}) \tag{2}$$

$$\text{TNR} = \text{Precision} = \text{TN} / (\text{FP} + \text{TN}) \tag{3}$$

$$\text{FNR} = \text{FN} / (\text{TP} + \text{FN}) \tag{4}$$

$$\text{FPR} = \text{FP} / (\text{FP} + \text{TN}) \tag{5}$$

where TP, TN, FP, and FN are the number of correct predictions for positive and negative subjects, and the number of incorrect predictions for positive and negative subjects, respectively. To evaluate these evaluation indices, we divided the measured data of each subject into training data (90%) for supervised learning and test data (10%) for evaluation.

The training and validations were executed using Windows 10 Pro personal computer (CPU: Intel Core i9, Memory: 192 GB, SSD: 1 TB and GPU: NVIDIA GeForce RTX 2080Ti). Following Python libraries were used to

construct machine-learning models: scikit-learn for KNN, LR, DT, RF, SVM and GBRT/DT, Keras and Tensorflow for NN, and XGBoost for Adaboost.

Experimental results

Figure 5 shows the R^2 score and MAE for each regressor. All regressors achieved a R^2 score exceeding 0.9, but the MAE ranged from 0.844 to 2.491. The SVM regressor had large variations of low to high level of CNR. The KNN regressor achieved high R^2 score and MAE was the best in all regressors, but the estimation errors occurred on low level CNR. The RF, GBRT, Adaboost and NN regressors had good linearity, of which the GBRT regressor was the highest with R^2 score of 0.995 and MAE of 0.844.

Figure 6 shows the confusion matrix for each classifier and depicts accuracy (ACC) and recall. All classifiers have similar results and achieved a higher accuracy exceeding 95% and a high recall exceeding 98%, of which

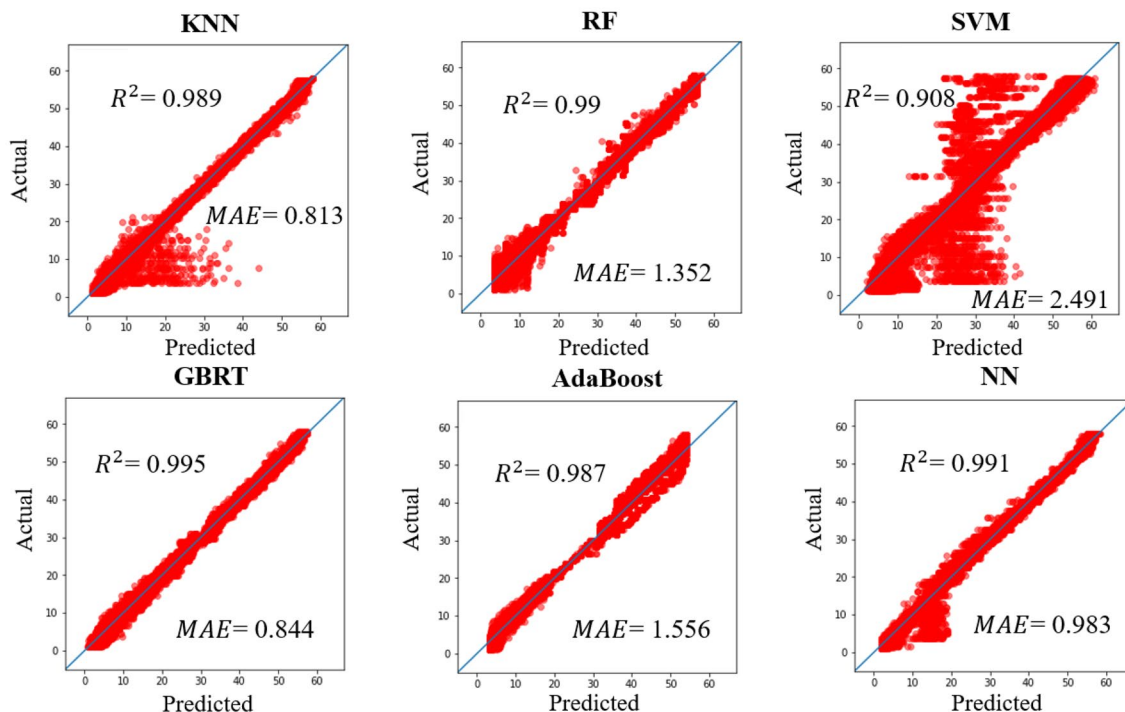


Figure 5. Results of the regression analysis.

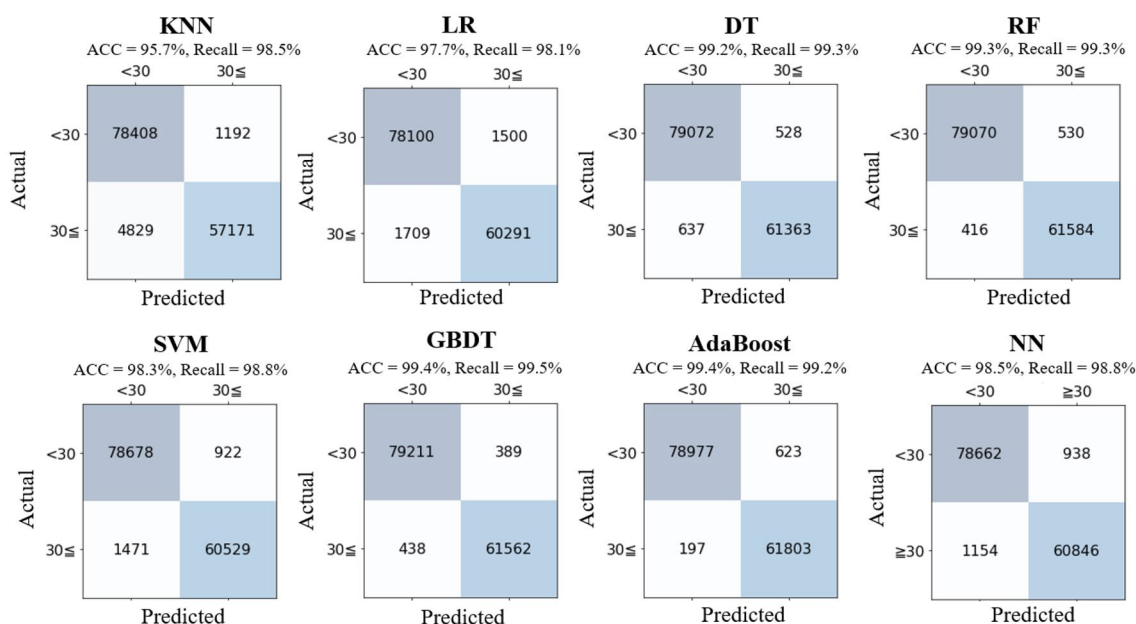


Figure 6. Results of the classification analysis.

the GBDT classifier was the best (ACC = 99.4%, recall = 99.5%). From the point of view of the risk management, overlooking of low level CNR may invoke poor reception of WMT. It is desirable to have a lower value of FN, hence, making GBDT the best classifier.

Adequacy and limitations

The CNR of WMT (3–50 dB) was reported at the Japanese University Hospital ward²⁸ and 6–61 dB at the simulated ward of the university department²⁹. Our training dataset approximately covers these CNR values. However, we reproduced various conditions of CNR obtained by varying the amplitude of both the WMT signal and BGN, indicating that our dataset covers cases of good reception with no EMI factor and the worst conditions of BGN increase.

In this study, we used a low-performance SDR device as a receiver to measure WMT signals. However, this SDR can capture a low amplitude signal of approximately –120 dBm; hence, making it sufficient to measure WMT signals at actual hospitals.

In our learning model, the GBRT regressor was the best and could estimate CNR within the error range of 1%. This high-precision estimator can provide a detailed survey of the electromagnetic environment in hospitals. For example, it could be useful for maintenance before or after replacing radio-receiving equipment, such as antennas and amplifiers. Furthermore, the GBDT classifier, which was our model's best accuracy, was sufficient in determining whether the CNR exceeded 30 dB. This model is promising for screening poor reception of WMT for periodic investigation in hospitals. Notably, managing the electromagnetic environment is important for the safe operation of medical devices, including WMT³⁰. However, most hospitals have generally been short staffed in the management of EMC. Our learning models are efficient in complementing the lack of skills, manpower, and specific instruments in clinical settings.

In this study, we targeted only the Japanese WMT, which uses the frequency of 400 MHz band. However, every country or region has different allocated frequency bands for WMT. For instance, Japan uses 400 MHz bands, while the US and EU use 600 MHz and 1400 MHz bands respectively^{15,31}. However, the specifications of both Japanese and US or EU WMT systems are almost the same: the transmitting power (1 mW), modulating scheme (frequency shift keying), and channel bandwidth (12.5 kHz). As the carrier frequency bands of the US and EU WMTs differ from that of Japan, but with the communication system being the same, we can acquire time-domain waveforms using the same measurement and can estimate CNR using our learning model.

Moreover, our datasets were collected from measurements by wired setting, but WMT signals are propagated in the air in actual settings. However, we cannot change the setting of the output power of the WMT transmitter in the body. But to reproduce and capture the various conditions of signal levels, we selected a wired setting that uses a TEM cell and variable attenuator. In clinical settings, WMT signals may vary due to the following reasons: reflection and diffraction on the wall, ceiling and flooring and the patient's body movement. However, as described earlier, our dataset covers low to high level CNR. If the WMT signal was varied broadly due to these effects, we can use the worst value as CNR.

We used Gaussian noise to increase BGN. In our previous study, we approximated most LED noise as Gaussian owing to band-limitation effect of the WMT receiver⁷. We intended to increase BGN as the effect of LED noise on WMT. However, some LED noise has sequential or impulsive characteristics, with a cycle of 50 Hz derived from the Japanese mains power supply, even in the band-limited reception³². This sequential noise causes approximately 3 dB worth of receiver sensitivity compared to LED noise, which can be approximated as Gaussian noise. On the other hand, by focusing on the highest position of the noise amplitude and broadening it, we can approximate this position as Gaussian noise even if the measured waveform has a sequential or impulsive nature. Therefore, our measured data also covers the increase in BGN caused by sequential and impulsive characteristic noise.

Discussion

In this study, we presented novel estimation technique for the CNR of WMT using machine-learning. Similar research in the estimating of signal to noise ratio (SNR) of wireless signals has been reported. Kojima reported that SNR was estimated by artificial NN, but this estimation was targeted to broad band communication such as wireless local area network of OFDM signal with a bandwidth of 20 MHz²⁶. On the other hand, we targeted narrow band communication of WMT with a bandwidth of 12.5 kHz. Xie reported other approach of SNR estimation that uses constellation diagrams of wireless signals and convolutional NN²⁷. However, we used time domain waveform of WMT signals instead of constellation diagrams for estimating CNR. Therefore, our approach is different from these past studies.

The major features of our method are the ease of estimation and the low cost in estimating CNR of WMT. We simultaneously measured and automatically estimated CNR at high accuracy. No prior skills or knowledge on electromagnetic waves and wireless communications are required. Moreover, we used a less expensive SDR dongle that costs approximately \$30 in substitution for a spectrum analyzer to measure the electromagnetic environment. The cost of a stand-alone spectrum analyzer usually exceeds \$1000; that of the USB-connected type exceeds \$400, but it is necessary to personal computers with a certain level of specification. The SDR dongle used in this study did not require a high-performance computer. Using a single-board computer such as Raspberry Pi as a control device, the SDR dongle was satisfactory for the measurement, and the total cost of our system was estimated as \$100–120. A single-board computer with a mounted graphic processing unit, such as NVIDIA Jetson Nano, is suitable for operating our learning model. As an alternative approach, our machine-learning models can be installed in the WMT receiver. In this case, no other computer is needed for connecting SDR or spectrum analyzers. However, existing radio-receiving equipment was used for the measurement. For future work, we propose installing our learning models on both single-board computers and WMT receivers.

Conclusion

We investigated a machine-learning model for estimating the CNR of WMT and found that GBRT was the best regressor and could estimate CNR within the error range of 1%. Also, GBDT was the best to classify whether the CNR exceeded 30 dB. Our proposed method evaluates the electromagnetic environment using a simplified, automated, and low-cost approach.

Data availability

The datasets used and/or analyzed during the current study available from the corresponding author on reasonable request.

Received: 12 September 2022; Accepted: 8 March 2023

Published online: 13 March 2023

References

1. Electromagnetic Compatibility Conference Japan (2022) Results of a survey on promoting proper use of radio waves at the medical institutions. https://www.emcc-info.net/medical_emc/pdf/22-300-mediemc-activityreports_2021.pdf.
2. Ishida, K., Wu, I., Gotoh, K. & Matsumoto, Y. Electromagnetic compatibility of 400 MHz radio communications in hospitals: Safety management of wireless medical telemetry. *J. Med. Syst.* **44**(9), 154. <https://doi.org/10.1007/s10916-020-01629-z> (2020).
3. Ishida, K. The simple approach of electromagnetic environment measurement methods in hospital. *Trans. Jpn. Soc. Med. Biol. Eng.* **59** Annual, 710–712. <https://doi.org/10.11239/jmsbe.Annual59.710> (2021).
4. Ishida, K., Arie, S., Wu, I., Gotoh, K. & Matsumoto, Y. Impact of LED lamp noise on receiver sensitivity of wireless medical telemetry system. *IEICE ComEx* **7**(11), 421–426. <https://doi.org/10.1587/comex.2018XBL0096> (2018).
5. Otsuka, T. Pitfalls of using medical machines on the wards: In case of wireless biomedical monitoring system. *JJMI* **75**(11), 822–827 (2005).
6. Fujii, K., Kishimoto, K. & Inoue, M. Fundamental study of quantitative evaluation of radio wave output of wireless medical telemetry transmitters operable in medical field. *GJMR-K Interdiscip.* **20**, 5–10 (2020).
7. Ishida, K., Wu, I., Gotoh, K. & Matsumoto, Y. Evaluation of electromagnetic noise emitted from light-emitting diode (LED) lamps and compatibility with wireless medical telemetry service. *IEICE Trans. Commun.* **E103-B**(6), 637–644. <https://doi.org/10.1587/transcom.2019HMP0003> (2020).
8. Electromagnetic Compatibility Conference Japan (2021) Guidance for using an electric wave safe and safely in a hospital.
9. Hanada, E., Ishida, K. & Kudou, T. Newly identified electromagnetic problems with medical telemeter systems. *Prz. Elektrotech.* **94**(2), 21–24. <https://doi.org/10.15199/48.2018.02.06> (2018).
10. Ishida, K. Study of electromagnetic interference caused by passive intermodulation of wireless medical telemetry services. *JJMI* **92**(1), 2–13. <https://doi.org/10.4286/jjmi.92.2> (2020).
11. Fujii, K., Ohno, Y., Kido, M., Ishida, K. & Jeong, H. Effect of wandering sensing systems on wireless medical telemetry systems. *Jpn. J. Med. Inf.* **38**(6), 321–336 (2018).
12. Ishida, K. Study of spectrum analyzer installed in wireless medical telemetry receiver. *JJMI* **90**(3), 237–244. <https://doi.org/10.4286/jjmi.90.237> (2020).
13. Ulversoy, T. Software defined radio: Challenges and opportunities. *IEEE Commun. Surv. Tutor.* **12**(4), 531–550 (2010).
14. Ishigami, S. *et al.* A new method of interference evaluation between an ultrawideband system and a wireless LAN using a gigahertz transverse electromagnetic cell. *IEEE Trans. Electromagn. Compat.* **52**(3), 737–744. <https://doi.org/10.1109/TEM.2010.2042959> (2010).
15. Association of Radio Industries and Businesses (2015) STD-21 ed.3.0, Medical telemeter radio equipment for specified low-power radio station.
16. McFee, B., Raffel, C., Liang, D., Ellis, D. P. W., McVicar, M., Battenberg, E. & Nieto, O. Librosa: Audio and music signal analysis in Python. IN *Proceedings of the 14th Python in Science Conference* 18–25. <https://doi.org/10.25080/Majora-7b98e3ed-003> (2015).
17. Sahidullah, M. & Saha, G. Design, analysis and experimental evaluation of block based transformation in MFCC computation for speaker recognition. *Speech Commun.* **54**(4), 543–565. <https://doi.org/10.1016/j.specom.2011.11.004> (2012).
18. Evelyn, F., & Joseph, L. H. Discriminatory Analysis. Nonparametric Discrimination: Consistency Properties. *USAF School of Aviation Medicine*, Randolph Field, Texas (1951).
19. Kleinbaum, D. G. & Klein, M. *Logistic Regression* (Springer, 2002). <https://doi.org/10.1007/978-1-4419-1742-3>.
20. Quilan, L. R. Simplifying decision trees. *Int. J. Man.-Mach. Stud.* **27**, 221–234. [https://doi.org/10.1016/S0020-7373\(87\)80053-6](https://doi.org/10.1016/S0020-7373(87)80053-6) (1987).
21. Breiman, L. Random forests. *Mach. Learn.* **45**, 5–32. <https://doi.org/10.1023/A:1010933404324> (2001).
22. Cortes, C. & Vapnik, V. Support-vector networks. *Mach. Learn.* **20**(2), 273–297. <https://doi.org/10.1007/BF00994018> (1995).
23. Natekin, A. & Knoll, A. Gradient boosting machines, a tutorial. *Front. Neurobot.* **7**, 21. <https://doi.org/10.3389/fnbot.2013.00021> (2013).
24. Kégl, B. The return of AdaBoost. MH: Multi-class Hamming trees. [arXiv:1312.6086](https://arxiv.org/abs/1312.6086) (arXiv preprint). <https://doi.org/10.48550/arXiv.1312.6086> (2013).
25. Rafiq, M. Y., Bugmann, G. & Easterbrook, D. J. Neural network design for engineering applications. *Comput. Struct.* **79**(17), 1541–1552. [https://doi.org/10.1016/S0045-7949\(01\)00039-6](https://doi.org/10.1016/S0045-7949(01)00039-6) (2001).
26. Kojima, S., Maruta, K. & Ahn, C. J. Adaptive modulation and coding using neural network based SNR estimation. *IEEE Access* **7**, 183545–183553. <https://doi.org/10.1109/ACCESS.2019.2946973> (2019).
27. Xie, X., Peng, S. & Yang, X. Deep learning-based signal-to-noise ratio estimation using constellation diagrams. *Mob. Inf. Syst.* **2020**, 8840340. <https://doi.org/10.1155/2020/8840340> (2020).
28. Kayano, I. *et al.* Novel channel management of wireless medical telemeters based on simulation and actual measurement of electromagnetic environment in a hospital. *JJMI* **91**(5), 411–421. <https://doi.org/10.4286/jjmi.91.411> (2021).
29. Kawabe, M., Kobayashi, N. & Kano, T. Development of management support system for evaluating the electromagnetic environment of wireless medical telemetry. *JJMI* **91**(6), 499–509 (2021).
30. Ishida, K. *et al.* Evaluation of electromagnetic fields in a hospital for safe use of electronic medical equipment. *J. Med. Syst.* **40**(3), 46. <https://doi.org/10.1007/s10916-015-0411-3> (2016).
31. Federal Communications Commission (1999) Wireless Medical Telemetry Service (WMTS).
32. Ishida, K., Arie, S., Wu, I., Gotoh, K., & Matsumoto, Y. Evaluation of Electromagnetic Noise Radiated from Tube-type LED Lamps and Its Effect on Wireless Medical Telemetry Systems. In *Proceedings of the EMC Europe 2019*.890–895. <https://doi.org/10.1109/EMCEurope.2019.8872012> (2019).

Acknowledgements

This work was supported by JSPS KAKENHI Grant Number JP19K19371.

Author contributions

K.I. conceptualized the study. K.I. measured data and investigated supervised machine-learning. K.I. wrote the main manuscript.

Competing interests

The author declares no competing interests.

Additional information

Correspondence and requests for materials should be addressed to I.K.

Reprints and permissions information is available at www.nature.com/reprints.

Publisher's note Springer Nature remains neutral with regard to jurisdictional claims in published maps and institutional affiliations.



Open Access This article is licensed under a Creative Commons Attribution 4.0 International License, which permits use, sharing, adaptation, distribution and reproduction in any medium or format, as long as you give appropriate credit to the original author(s) and the source, provide a link to the Creative Commons licence, and indicate if changes were made. The images or other third party material in this article are included in the article's Creative Commons licence, unless indicated otherwise in a credit line to the material. If material is not included in the article's Creative Commons licence and your intended use is not permitted by statutory regulation or exceeds the permitted use, you will need to obtain permission directly from the copyright holder. To view a copy of this licence, visit <http://creativecommons.org/licenses/by/4.0/>.

© The Author(s) 2023